AGU PUBLICATIONS

JGR

Journal of Geophysical Research: Biogeosciences

RESEARCH ARTICLE
10.1002/2014JG002804

Key Points:
- Plot level scaling of evaporation from sap flux evaluated with eddy flux
- Disturbance changes intradaily transpiration dynamics
- Hydraulic strategy causes species-specific transpiration differences

Supporting Information:
- Text S1 and Table S1

Correspondence to:
A. M. Matheny,
Matheny.44@osu.edu

Citation:
Matheny, A. M., et al. (2014), Species-specific transpiration responses to intermediate disturbance in a northern hardwood forest, *J. Geophys. Res. Biogeosci.*, *119*, 2292–2311, doi:10.1002/2014JG002804.

Received 15 SEP 2014
Accepted 25 NOV 2014
Accepted article online 4 DEC 2014
Published online 23 DEC 2014

Species-specific transpiration responses to intermediate disturbance in a northern hardwood forest

Ashley M. Matheny[1], Gil Bohrer[1], Christoph S. Vogel[2], Timothy H. Morin[1], Lingli He[3], Renato Prata de Moraes Frasson[1], Golnazalsadat Mirfenderesgi[1], Karina V. R. Schäfer[4], Christopher M. Gough[5], Valeriy Y. Ivanov[3], and Peter S. Curtis[6]

[1]Department of Civil, Environmental, and Geodetic Engineering, Ohio State University, Columbus, Ohio, USA, [2]University of Michigan Biological Station, Pellston, Michigan, USA, [3]Department of Civil and Environmental Engineering, University of Michigan, Ann Arbor, Michigan, USA, [4]Department of Biological Sciences, Department of Earth and Environmental Science, Rutgers University, Newark, New Jersey, USA, [5]Department of Biology, Virginia Commonwealth University, Richmond, Virginia, USA, [6]Department of Evolution, Ecology, and Organismal Biology, Ohio State University, Columbus, Ohio, USA

Abstract Intermediate disturbances shape forest structure and composition, which may in turn alter carbon, nitrogen, and water cycling. We used a large-scale experiment in a forest in northern lower Michigan where we prescribed an intermediate disturbance by stem girdling all canopy-dominant early successional trees to simulate an accelerated age-related senescence associated with natural succession. Using 3 years of eddy covariance and sap flux measurements in the disturbed area and an adjacent control plot, we analyzed disturbance-induced changes to plot level and species-specific transpiration and stomatal conductance. We found transpiration to be ~15% lower in disturbed plots than in unmanipulated control plots. However, species-specific responses to changes in microclimate varied. While red oak and white pine showed increases in stomatal conductance during postdisturbance (62.5 and 132.2%, respectively), red maple reduced stomatal conductance by 36.8%. We used the hysteresis between sap flux and vapor pressure deficit to quantify diurnal hydraulic stress incurred by each species in both plots. Red oak, a ring porous anisohydric species, demonstrated the largest mean relative hysteresis, while red maple, bigtooth aspen, and paper birch, all diffuse porous species, had the lowest relative hysteresis. We employed the Penman-Monteith model for LE to demonstrate that these species-specific responses to disturbance are not well captured using current modeling strategies and that accounting for changes to leaf area index and plot microclimate are insufficient to fully describe the effects of disturbance on transpiration.

1. Introduction

Evapotranspiration (*ET*) accounts for 60–95% of precipitated water in terrestrial ecosystems, comprising the one of the largest components of the terrestrial hydrologic cycle [*Fisher et al.*, 2005; *Ford et al.*, 2007; *Jasechko et al.*, 2013; *Katul et al.*, 2012]. Transpiring vegetation recycles ~62,000 km^3 of water, while sequestering ~130 Gt of carbon annually at the global scale [*Jasechko et al.*, 2013]. Transpiration couples the carbon, energy, and water cycles and acts as the principal feedback between the land surface and atmosphere. It is therefore crucial to understand its dynamics. With global and regional temperature increases and a potential rise of the variation in regional precipitation patterns, the ability to accurately simulate transpiration is essential to predicting land surface-climate change feedbacks in terms of heat, water, and carbon exchange [e.g., *Allen et al.*, 2010; *Choat et al.*, 2012; *Wu et al.*, 2012].

Disturbance plays a major role in determining forest structure, composition, and carbon (C), nitrogen (N), and water cycling [*Pan et al.*, 2011]. Nonstand replacing disturbances, often called intermediate disturbances, occur naturally via species-specific pest infestation [e.g., *Herms and McCullough*, 2014; *Simard et al.*, 2012], strong storms and wind throws [e.g., *Uriarte et al.*, 2012], drought [e.g., *Huang and Anderegg*, 2012; *McDowell et al.*, 2008; *Royer et al.*, 2010], and ecological succession [e.g., *Gough et al.*, 2013; *Hardiman et al.*, 2013] and anthropogenically via fire management and biomass removals [e.g., *Royer et al.*, 2010; *Stephens et al.*, 2009] and selective logging [e.g., *Asase et al.*, 2014; *Asner et al.*, 2004]. These disturbances impact canopy structure at a diffuse spatial scale ranging from one to several tree crowns per hectare, and may be distributed over

large regional spatial domains. Disturbances at this scale will impact the heterogeneity of light attenuation through the canopy [*Hardiman et al*., 2013; *Schnitzer et al*., 2012] and the canopy microclimate, including wind speed, turbulent mixing, humidity, temperature, and soil moisture under the canopy [*Asase et al*., 2014; *Bohrer et al*., 2009; *Forrester et al*., 2012; *He et al*., 2013; *Maurer et al*., 2013]. These variables directly affect photosynthesis, canopy evaporative demand, and soil water availability, thereby influencing transpiration.

Ultimately, the interaction between the hydrodynamic traits of trees, such as stomatal response to vapor pressure deficit and leaf water potential, the root response to soil water deficit, the conductivity and structure of the xylem system, and environmental conditions at the tree crown determine the way in which individual trees respond to microclimatic changes following disturbance. The responses of photosynthesis and transpiration to disturbance may be driven in a large part by dynamic changes to stomatal conductance and by spatial variation in leaf distribution. Given the nonlinear nature of leaf stomatal conductance and transpiration, special attention should be paid to the mechanistic physiological properties that control them. Nonetheless, a majority of current land surface models represent this type of intermediate disturbance through a change in overall leaf area index (LAI), the only manner through which canopy structure is represented in coarse-scale, largely big-leaf or two-layer models (e.g., CanIBIS [*Kucharik et al*., 2000], SiB2 [*Sellers et al*., 1995], and BiomeBGC [*Running and Coughlan*, 1988]). Although changes to LAI will affect simulated photosynthesis and transpiration, changes in LAI alone may not capture the observed effects of intermediate disturbance on transpiration.

Tree growth following intermediate disturbance will result in structural changes including sapwood-to-leaf area ratio, LAI, and the mean and variability of tree height [*Dietze et al*., 2008]. These factors influence tree C uptake and water flux, and it is unlikely that all species will respond to these changes in the same manner [e.g., *Chapin*, 2003; *Ewers et al*., 2008; *Moore et al*., 2004; *O'Brien et al*., 2004; *Schäfer et al*., 2013]. Further studies have described numerous differences among species responses to the same environmental conditions on the basis of hydraulic strategy and functional type [e.g., *Ford et al*., 2011; *McCulloh et al*., 2012; *Thomsen et al*., 2013]. Incorporating differences in species-specific controls over transpiration in models may improve the prediction of whole forest transpiration, and how it responds to disturbance-induced differences in microclimate, canopy structure, and species composition.

Following intermediate disturbance, as forcing conditions and canopy structure around the tree change, internal water storage levels, xylem water potential, and stomatal conductance may also change accordingly. The imbalance between the rates of water demand in the leaf and water supply from the soil imposes hydrodynamic limitations on stomatal conductance [*Bohrer et al*., 2005; *Damour et al*., 2010; *McCulloh and Sperry*, 2005; *Tyree and Sperry*, 1989]. Hydraulic limitations have recently been linked to the hysteretic relationship between transpiration (or stomatal conductance) and vapor pressure deficit (VPD) [*Matheny et al*., 2014; *Novick et al*., 2014; *O'Brien et al*., 2004; *Unsworth et al*., 2004; *Verbeeck et al*., 2007a; *Zhang et al*., 2014]. For a given level of atmospheric VPD and soil moisture, plants transpire more during the morning hours, when internal water storage is high, than they do for the same *VPD* in the afternoon-evening hours, when within-plant water storage may have become depleted. Thus, when plotting transpiration throughout the day as a function of VPD, a hysteretic "loop" is created. This hysteresis is related in part to the time lag between daily maximal light and daily maximal VPD conditions, but it is also driven by the daily hydrodynamic cycle and the depletion of water storage within the plant. The area enclosed by this loop, can thus be indicative of the relative change in plant water status throughout the day and the degree of hydrodynamic stress incurred by the plant.

The hydrodynamic processes that drive the daily hysteresis of transpiration operate at a fast, intradaily time scale and at the spatial scale of a single tree, and when aggregated over many trees, can change the overall diurnal distribution of transpiration and stomatal conductance at the plot level. These processes, and their interactions with changes to canopy structure and species composition could also accumulate to affect total transpiration over longer (daily-seasonal-annual) time scales by affecting water use efficiency and the effective degree of daily stomata-closing stresses the trees experience post disturbance. By analyzing and understanding these fast daily dynamics rather than longer-term periods (monthly) or periods of drought stress, it may be possible to improve modeling of transpiration at the subdaily time step [*Thompson et al*., 2011] as well as to show more realistic coupling between hydrodynamic phenomena and gross primary productivity in land surface models [*Fatichi and Ivanov*, 2014].

We used a large-scale experiment to examine the response of tree and plot-scale transpiration to changes in canopy structure resulting from an intermediate disturbance. This study utilized meteorological, eddy covariance, sap flow, and soil moisture observations in two forest plots. Our experiment was composed of a control plot in a mixed, deciduous, mature (~90 years old), early-middle successional forest in Northern Michigan, and a nearby treatment plot, where all early successional aspen and birch trees were killed by stem girdling to represent an intermediate disturbance that accounted for roughly 35% of leaf area in the predisturbance forest [*Hardiman et al*., 2013]. This disturbance has resulted in a successional shift into a middle-late successional forest structure, dominated by red maple, red oak, and white pine. We monitored the transpiration response of trees in the disturbed plot and the undisturbed control. We hypothesized that

1. Species with different hydraulic strategies and xylem structure, i.e., red oaks, red maples, and white pines, would demonstrate different capacities to increase transpiration following disturbance.
2. Disturbance-related changes to external physical drivers of transpiration would influence the diurnal pattern of transpiration more strongly in some species than in others. This would cause increases in afternoon hydrodynamic stress and stomata closure in relatively isohydric species such as red maple during most of the growing season when precipitation at our site is not limiting.
3. Diurnal hydraulic stress, expressed as the hysteresis of the transpiration curve, would be consistently greater in anisohydric species than in similarly sized isohydric species.
4. As a result of changes to microclimate and species composition, plot level transpiration and stomatal conductance in postdisturbance plots would be significantly different from plot level transpiration in undisturbed plots. This difference would not be simply scaled by the leaf areas of the two plot types, indicating that changes in LAI alone are not sufficient to represent disturbance in land surface models.

2. Methods

2.1. Site Description

This study was completed at the University of Michigan Biological Station (UMBS) located in northern, Lower Michigan, USA. The site receives 805 mm of mean annual precipitation and has an annual average temperature of 6.8°C. Soils consist of well drained Haplorthods of the Rubicon, Blue Lake or Cheboygan series that are 92.2% sand, 6.5% silt and 0.6% clay [*Nave et al*., 2011]. We conducted our study in two adjacent forest plots surrounding two Ameriflux-affiliated eddy covariance flux stations (http://ameriflux.lbl.gov/). The experiment and site layout are described in detail in *Gough et al*. [2013]. While neither of our two forest plots is physically bounded, we considered the control plot area to be the 180 ha area composing 99% of the flux footprint of the primary eddy covariance tower. The experimental plot consists of a 39 ha plot surrounding the secondary eddy covariance tower, where a manipulation treatment was enacted to accelerate succession. Because of the treatment plot's smaller size, it typically contributes 70–90% of the flux footprint. To account for this, we further normalized plot level eddy covariance measurements from the treatment plot (see "Eddy covariance measurements" below). Within each plot, we had one large 60 m diameter and 80 (in the control) and 22 (in the treatment) 16 m census plots, where the diameters at breast height (DBH) of all trees larger than 8 cm were measured (see "Scaling tree level sap flow to plot level transpiration" below).

The control plot (45°33′35″N, 84°42′48″W, elevation 236 m) is dominated by early successional bigtooth aspen (*Populus grandidentata*) and paper birch (*Betula papyrifera*). As these early successional trees begin to decline, later successional species such as red oak (*Quercus rubra*), red maple (*Acer rubrum*), white pine (*Pinus strobus*), American beech (*Fagus grandifolia*), and sugar maple (*Acer saccharum*) are beginning to comprise a more significant portion of the stand basal area. Mean canopy height is approximately 25 m, average tree age is ~90 years, mean peak LAI is ~3.9 $m^2\ m^{-2}$, and average stem density is ~750 trees ha^{-1} (for trees with diameter at breast height ≥ 8 cm) [*Gough et al*., 2010]. Flux, meteorological, and plot level biological data are available from the Ameriflux database, under the site-ID US-UMB.

The treatment plot (45°33′45″N, 84°41′51″W, elevation 239 m) was designed as part of the Forest Accelerated Succession ExperimenT to test the effects of intermediate disturbance and ecological succession on forest biogeochemistry. In 2008, all aspen and birch within the treatment plot were stem girdled to induce mortality within 2–4 years. The remaining canopy is dominated by red oak, red maple, white pine, and American

Table 1. List of Instrumented Sap Flux Trees for Each Plot. Ranges for DBH, Height, and Projected Crown Area for All Trees

	n	DBH (cm)	Height (m)	Crown Area (m^2)	Sapwood Depth (cm)	LAI (m^2/m^2)	Leaf Area per Xylem Area (m^2/m^2)
				Control			
Red oak	10	21.7–37.2	11.1–26.7	23.2–179.6	3.0–5.6	0.99	5400
Red maple	8	11.9–22.3	9.6–17.4	20.2–82.0	3.8–9.3	0.84	2000
White pine	8	6–32.5	4.2–20.4	5.9–24.1	1.7–3.6	0.69	3500
Bigtooth aspen	8	16.4–32.5	13.5–22.1	10.4–49.0	6.8–12.8	0.94	970
Paper birch	8	10.4–25	10.1–16.0	11.1–79.5	4.6–10.0	0.20	1400
				Treatment			
Red oak	10	8.2–41.6	11.0–25.5	3.6–88.1	0.8–6.8	1.11	3300
Red maple	12	7.9–28.4	9.8–25.7	4.9–81.7	2.8–10.6	1.23	2900
White pine	10	7.2–30.5	5.8–22.9	5.3–25.9	2.0–5.1	0.45	820
American beech	10	12.2–22.2	11.2–25.5	25.9–89.8	2.7–4.0	0.75	12000

beech.Before the experimental girdling, the treatment and control plots (about 1.2 km away) were similar in forest composition, structure, soil, and meteorological conditions. In 2008, the control and treatment plots differed in growing season mean latent heat flux by less than 1.5 W m^{-2}. Flux, meteorological, and plot level biological data are available from the Ameriflux database, under the site-ID US-UMd.

2.2. Experimental Approach

We combined long-term plot level and individual tree level observations of transpiration, sap flow, soil moisture, and other environmental conditions to test our hypotheses and isolate species-specific differences in transpiration and hydrodynamic regulation of stomatal conductance. We scaled measured values of sap flux from 84 trees to the equivalent plot level transpiration and evaluated our estimates using eddy covariance measurements of latent heat flux. We then used sap flux observations to estimate stomatal conductance and demonstrate differences in daily patterns of stomatal closure between species and size classes of trees. Similarly, we used the statistics of daily hysteresis of the transpiration-VPD curve to quantify the degree of short-term (intradaily) hydraulic stress each species incurred and analyzed the relationship between the extent of hysteretic stress and environmental forcings, particularly VPD and soil water potential. Finally, we employed the Penman-Monteith (PM) model for transpiration as a null hypothesis to account for the effects of all environmental forcings on evapotranspiration, with the exception of soil water potential and tree hydrodynamics. We compared the residuals between predictions from the PM model and observed daily transpiration to determine the effects of species, size, and hydraulic strategy on actual transpiration under different soil water potential conditions. The formulations and more detailed explanations for these analyses are provided in the following sections.

2.3. Sap Flux Measurements

We observed and quantified the forest's response to disturbance by monitoring sap flux in the experimental and control forest plots and determined whether the different postdisturbance species composition affected transpiration and as well as whether the lessened competition for resources resulted in increased transpiration at the treatment plot. In 2011 and 2012, 30 trees in each plot were instrumented with *Granier* [1987] style thermal dissipation probes to continuously measure sap flux density (J_{sji}). Data were recorded every minute and averaged to half-hourly time steps. In 2013, additional sensors were added for a total of 42 instrumented trees per plot ($n = 84$). Trees were selected to represent the characteristic canopy-dominant species and sizes (i.e., height and diameter) for each plot (Table 1). Pairs of 20 mm long, self-manufactured probes were inserted into the sapwood at breast height (1.37 m) on the north facing side of the tree with a vertical separation of ~10 cm. For all trees where sapwood depth was less than 2 cm, the *Clearwater et al.* [1999] correction was applied. Sap flux sensor data were processed using a baselining procedure to account for the daily maximum temperature of each sensor and times when the 2 h average VPD was lower than 0.5 kPa in order to account for nocturnal recharge flux [*Oishi et al.*, 2008]. No radial scaling information was available for our plots [*Phillips et al.*, 1996]. We therefore assumed that our sap flux measurements represent an average sap flux density through the entire conductive area.

Table 2. Species-Specific Allometric Factors for the Determination Sapwood Area (A_{si}, cm^2) on the Basis of DBH (cm) in Equation (1)

Species (n)	α_1	α_2	α_3	R^2	Reference
Red oak (14)	0	0.21	2.1838	0.95	
White pine (15)	0	1	1.7491	0.97	
American beech (15)	0	1.15	1.6946	0.91	
Bigtooth aspen (16)	0	0.77	1.868	0.97	*Bovard et al.* [2005]
Paper birch (12)	−112.21	17.17	1	0.98	*Bovard et al.* [2005]
Red maple (13)	−110.66	17.04	1	0.98	*Bovard et al.* [2005]

2.4. Sapwood Depth Measurements

Allometric equations relating diameter at breast height to sapwood area were developed for the main species (aspen, birch, and maple) at our site by *Bovard et al.* [2005]. An expansion of the *Bovard et al.* [2005] study was conducted during summer 2014 to determine allometric scaling relationships for red oak, white pine, and American beech. To develop these relationships, tree cores were taken at breast height and stained using a 2% solution of tetrazolium chloride (TTC) to determine the depth of hydroactive xylem. The results from all trees of the same species were fitted to an allometric equation (equation (1)) to describe the relationship between DBH and active xylem area (A_{si}). The species-specific parameters of the allometric equation (equation (1)) are listed in Table 2. Oak cores, for which the TTC assay gave ambiguous results, were further analyzed using a stereoscopic microscope to verify the results of the staining assay.

$$A_{si} = \alpha_{1s} + \alpha_{2s}\mathrm{DBH}_i^{\alpha_{3s}} \quad (1)$$

2.5. Scaling Tree Level Sap Flow to Plot Level Transpiration

We measured the DBH and projected crown area of each tree in which we installed a sap flow sensor. Projected crown area was estimated using the perpendicular major and minor diameters of each crown as measured from the ground. Crown area was then calculated following the assumption that crowns tend to be roughly elliptical in shape. The observed sap flow rate per unit sapwood area was scaled to the total flow through the stem using the tree's sapwood area (A_{sji}) obtained from the DBH-A_s allometric relationships described above. We characterized three size bins defining small, medium, and large trees as having DBH of 6–10 cm, 10.1–20 cm, and >20 cm, respectively. Plot-scale total basal area for each species/size bin was determined using tree census data collected in 2010 (Figure 1), with further adjusted DBH values for each subsequent year. Adjusted DBH values were calculated on the basis of dendrometer measurements that provide continuous measurement of DBH at a subsample of the trees, $n = 933$ and 449 for the control and treatment plots, respectively [*Gough et al.*, 2008, 2013; . Incremental growth data for the study period is presented in Table 3. Trees instrumented with sap flow sensors were binned on the same species/size basis as the plot-scale histogram.

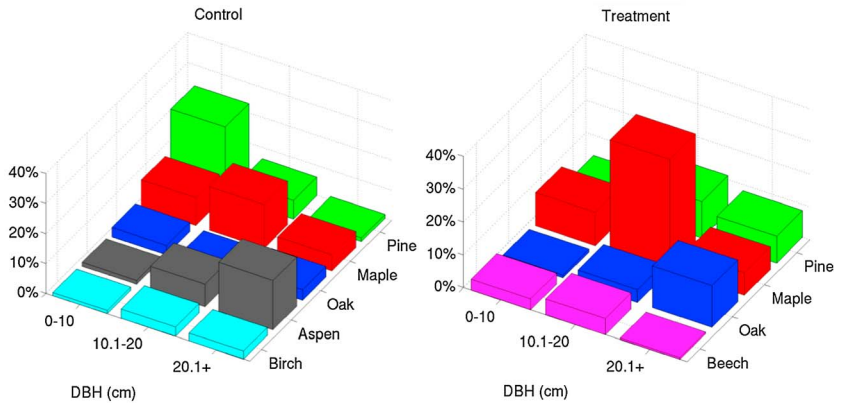

Figure 1. Species/size histograms for the total plot area (A_P) (75,649 and 29,003 m^2 in the control and treatment plots, respectively). Percent composition of total trees is displayed: 8974 trees were surveyed in the control and 2567 in the treatment plot.

Table 3. Incremental Growth Data for Each Study Species at the Control and Treatment Plots[a]

	Bole Area per Ground Area ($m^2\ ha^{-1}$)	Average Annual Increase	LAI	Average Annual Increase	Leaf Area per Sapwood Area	Average Annual Increase
			Control			
Red oak	3.7	2.1%	1.1	−7.6%	6029.4	−7.8%
Red maple	6.0	1.3%	0.9	1.1%	2161.8	3.6%
White pine	2.6	3.5%	0.7	−15.0%	4165.4	−15.2%
Bigtooth aspen	16.1	1.4%	0.9	9.4%	897.1	8.0%
Paper birch	2.4	0.5%	0.2	−2.3%	1365.8	−1.0%
			Treatment			
Red oak	7.1	2.3%	1.3	−6.1	3728.5	−5.5%
Red maple	5.7	2.0%	1.4	2.5%	3362.0	0.9%
White pine	5.5	2.1%	0.4	6.0%	771.1	3.0%
American beech	0.8	2.5%	0.4	32.5%	7946.1	28.6%

[a]Initial values are from 2011 and have units of $m^2\ m^{-2}$, unless specified otherwise.

Plot total sap flux equivalent transpiration (E_C, $W\ m^{-2}$) was computed as the sum of sap flux equivalent transpiration from all species (E_s) which is, in turn,

$$E_C = \sum_s E_s = \sum_s \sum_j E_{sj} \tag{2}$$

where here, and throughout the manuscript, subscript *i* represents individual tree in which sap flux was measured, *j* represents size bin, and *s* represents species. The sum of sap flux equivalent transpiration from all size bins within the species (E_{sj}) as calculated from the tree level observation of sap flux density per sapwood area (J_{sji}, $g\ m^{-2}_{sapwood}\ s^{-1}$):

$$E_{sj} = \frac{\sum_k A_{sjk}}{A_p} \lambda J_{sj} \tag{3}$$

$$J_{sj} = \left(\frac{1}{n_{sj}} \sum_i J_{sji} \right) \tag{4}$$

where λ is the latent heat of vaporization of water (2440 kJ/kg), A_{sjk} is the sapwood area of each tree of each size bin and species in the census plot. Here and throughout the manuscript, subscript *k* represents an individual tree within the census plot. n_{sj} is the number of trees where sap flow was observed for each species and size bin, and A_P is the total ground area of the plot.

Plot level total (J_C, $g\ m^{-2}_{sapwood}\ s^{-1}$) and species-specific sap flux per sapwood area (J_s, $g\ m^{-2}_{sapwood}\ s^{-1}$) were calculated as

$$J_C = \sum_s J_s \tag{5}$$

$$J_s = \frac{1}{\sum_j \sum_k A_{sjk}} \sum_j \left(\sum_k A_{sjk} \right) J_{sj} \tag{6}$$

Similarly, canopy transpiration per leaf area (E_L, $g\ H_2O\ m^{-2}_{leaf}\ s^{-1}$) was calculated from plot level sap flux using the plot level species-specific sapwood to leaf area ratio:

$$E_L = \sum_s E_{L,s} = \sum_s \sum_j E_{L,sj} \tag{7}$$

$$E_{L,sj} = \frac{\sum_k A_{sjk}}{A_{L,s}} J_{sj} \tag{8}$$

where $A_{L,s}$ is the plot level species-specific leaf area ($m^2_{leaf}\ m^{-2}_{ground}$) during each week of the growing season. Species-specific seasonal and maximum seasonal LAI for our site were measured by litter traps and optical

(LAI-2000, LI-COR Biosciences, Lincoln, NE) measurements in each plot, respectively. To account for changes in LAI throughout the course of the growing season, total canopy LAI optical measurements were conducted weekly during leaf out (April–May) and at the beginning of leaf senescence (late September to early October), and monthly during the rest of the growing season (June–September). Observations were made at six locations per plot and averaged at the plot level. Seasonal time series of LAI were normalized by peak seasonal LAI. Normalized LAI time series were multiplied by the species-specific LAI from the litter traps to create species-specific time series for each growing season. This time course of species-specific LAI was used to calculate $A_{L,s}$ in equation (8).

Similarly to sap flux, stomatal conductance per species (g_s) was calculated as the sum of stomatal conductance over all size classes for a particular species in each plot. Assuming strong coupling between the atmosphere and canopy [*McNaughton and Jarvis*, 1986], stomatal conductance for each species/size bin (g_{sj}) was calculated from $E_{L,sj}$ following *Phillips and Oren* [1998] using species-specific LAI and was converted to the units of mmol H_2O m_{leaf}^{-2} s^{-1} (following *Pearcy et al.* [1989]).

$$g_s = \sum_j g_{sj} \tag{9}$$

$$g_{sj} = \left(\frac{P * E_{L.sj}}{\rho_{air}(T)\frac{MW_{water}}{MW_{air}}VPD}\right) R\left(\frac{T_0}{T+T_0}\right)\left(\frac{P}{P_0}\right) \tag{10}$$

where P is atmospheric pressure (kPa), T is air temperature (°C), $\rho_{air}(T)$ is air density as a function of T (kg m^{-3}), and MW_{water} and MW_{air} are the molecular weights of water and air, respectively, (mol kg^{-1}), $R = 0.0446$ is the ideal gas constant adjusted for water vapor (mol mm^{-3}), $P_0 = 101.3$ is the standard sea level atmospheric pressure (kPa), and $T_0 = 273$ is the temperature conversion from °C to K. The final two terms in equation (10) correct for the effects of temperature and pressure on the volume of air. To reduce errors in calculated g_{sj}, periods when VPD < 0.6 kPa were excluded (following *Ewers and Oren* [2000]). A full derivation of equation (10) is provided in Text S1 in the supporting information.

2.6. Soil Water Potential Measurements

Soil moisture and temperature were recorded at four locations in each plot at depths of 5, 15, 30, and 60 cm, and at two locations in each plot at 100, 200, and 300 cm (Hydra probe SDI-12, Stevens Water Monitoring Systems, Inc., Portland, OR, USA) [*He et al.*, 2013]. All soil moisture data were corrected by adding an estimate of systematic bias (estimated to be ~0.03 m^3 m^{-3}). To eliminate sensor noise (± 0.001 m^3 m^{-3}), the soil moisture data were processed with a moving averaging window with a size of 10 h. Soil moisture values in each measurement depth at each plot were averaged (two to four measurements per plot, depending on depth). The soil water potential values (Ψ, mm) were estimated by using the *Van Genuchten* [1980] hydraulic parameterization with residual and saturation soil water contents $\theta_r = 0.04$ (m^3 m^{-3}) and $\theta_s = 0.45$ (m^3 m^{-3}). Soil hydraulic parameters were derived from pedotransfer functions using the percentages of sand, silt, and clay (92%, 7%, and 1%) for our plots [*He et al.*, 2013]. Ψ was then converted from units of millimeters to units of kilopascal.

2.7. Classification of "Wet" and "Dry" Days

Soil water potential at each depth was found to be highly correlated with soil water potential at every other depth in each plot. We selected Ψ at 30 cm (Ψ_{30cm}) for our analysis as it was the most strongly correlated with sap flux from the largest number of species in both plots. Soil conditions were characterized into three categorical levels on the basis of Ψ_{30cm}, representing the times when the soil was wettest, intermediately wet, and driest. Days for which the daily mean Ψ_{30cm} fell within the highest (least negative) 33% of the seasonal range of Ψ_{30cm} were considered "wet soil" days (−5 to −15 kPa). Similarly, in "dry soil" days the mean daily Ψ_{30cm} fell within the lowest (most negative) 33% (−25 to −35kPa), and "intermediate soil" refers to the middle 33% (−15 to −25 kPa). VPD was characterized into three categories in a similar manner, such that days with a daily mean VPD within the highest 33% of the seasonal VPD range were considered "high VPD" days, while days within the bottom 33% were considered "low VPD", and the intervening 33% were considered to have "intermediate VPD" conditions.

Table 4. Seasonal Means (± 1 SD) of Principal Environmental Conditions (Atmospheric Vapor Pressure Deficit (VPD), Air Temperature (Temp), and Soil Water Potential) for Control and Treatment Plots Across the 3 Year Observational Period

	VPD (kPa)	Temp (°C)	Soil Water Potential at 30 cm (kPa)
Control	0.70 ± 0.09	19.00 ± 0.63	−17 ± 3
Treatment	0.69 ± 0.10	18.49 ± 0.95	−13 ± 3

2.8. Eddy Covariance Measurements

In each plot, above-canopy meteorological conditions as well as CO_2 and H_2O fluxes were measured from towers. The control plot tower measurements were conducted at two levels, 46 m and 34 m. Tower-top observations at the treatment plot were conducted at 32 m. Radiation and precipitation data used in this study were only conducted at the higher level of the control tower but reflect the conditions in the entire site [*Gough et al*., 2013]. We used the air temperature, humidity, pressure, and fluxes from top level at each plot. Precipitation was measured using a tipping bucket rain gauge (TE-525, Texas Electronics, Dallas, TX, USA). Incoming photosynthetically active photon flux (PAR) was measured using a quantum PAR sensor (LI-190, LI-COR Biosciences, Lincoln, NE, USA). Air temperature and humidity were measured in each plot (HMP45g, Vaisala, Helsinki, Finland). Atmospheric pressure was measured by a pressure sensor (PTB101B, Vaisala, Helsinki, Finland). Observations from these sensors were recorded every 10 min. Latent heat flux was measured using the eddy covariance approach using closed-path infrared gas analyzers (LI7000, LI-COR Biosciences, Lincoln, NE, USA), which provide water vapor and CO_2 concentrations observations, and 3-D ultrasonic anemometers (CSAT3, Campbell Scientific, Logan, UT, USA) which provide high-frequency wind velocities and temperature measurements, all measured at 10 Hz [*Schmid et al*., 2003]. At each tower, the anemometer was located near the gas analyzer inlet.

Data from the sensors were despiked and spurious observations that were beyond the acceptable physical range or identified as outliers by exceeding 6 standard deviations above the mean of a 2 min moving window were removed. We also removed any observation that was marked by the sensors' built-in quality control indicators. These were typically flagging data during precipitation. Time series from the two sensors were aligned to correct for placement separation distance following the maximal covariance approach. The anemometer data were rotated in 3-D such that the half-hourly mean vertical wind speed was set to zero and the horizontal wind was aligned with the mean wind direction [*Finnigan*, 2004]. Temperature measurements from the sonic were corrected for crosswind velocity contamination, following *Kaimal and Gaynor* [1991] and their covariance with vertical wind provided the sensible heat flux. Seasonal averages of the principal meteorological conditions for each plot are presented in Table 4. Primary forcing conditions (precipitation, soil moisture, temperature, and incoming radiation) and latent heat flux for both plots from 2008 to 2013 are presented in Figure 2.

Latent heat flux was calculated from the covariance of water vapor concentration with vertical wind. A correction based on Webb-Pearman-Leuning [*Detto and Katul*, 2007; *Webb et al*., 1980] that included only the sensible heat flux term was applied to the latent heat flux to yield the final half-hourly above-canopy estimates of latent heat flux (LE). A spectral correction was applied to the water vapor flux measurements to account for volume averaging and signal dissipation in the sampling tube [*Massman*, 2000]. We used a threshold frictional velocity value (u_* filter, based on the approach of *Reichstein et al*. [2005]) to filter data when turbulent mixing was low. A detailed description of our eddy flux processing is reported in *Gough et al*. [2013]. We used a bilinear periodic approach [*Morin et al*., 2014] to gap-fill latent and sensible heat flux. We quantify our confidence in measured LE using the energy budget closure. The relative deficit in the energy budget (δ) can be approximated as:

$$\delta = \frac{\sum_{\text{season}} (R_n - \text{LE} - H - G)}{\sum_{\text{season}} R_n} \tag{11}$$

where R_n is net radiation (W m^{-2}), H is sensible heat flux (W m^{-2}), and G is ground heat flux (W m^{-2}) calculated following *Liebethal et al*. [2005]. To compute the total seasonal deficit in the energy budget, daily deficits were summed over the duration of the season.

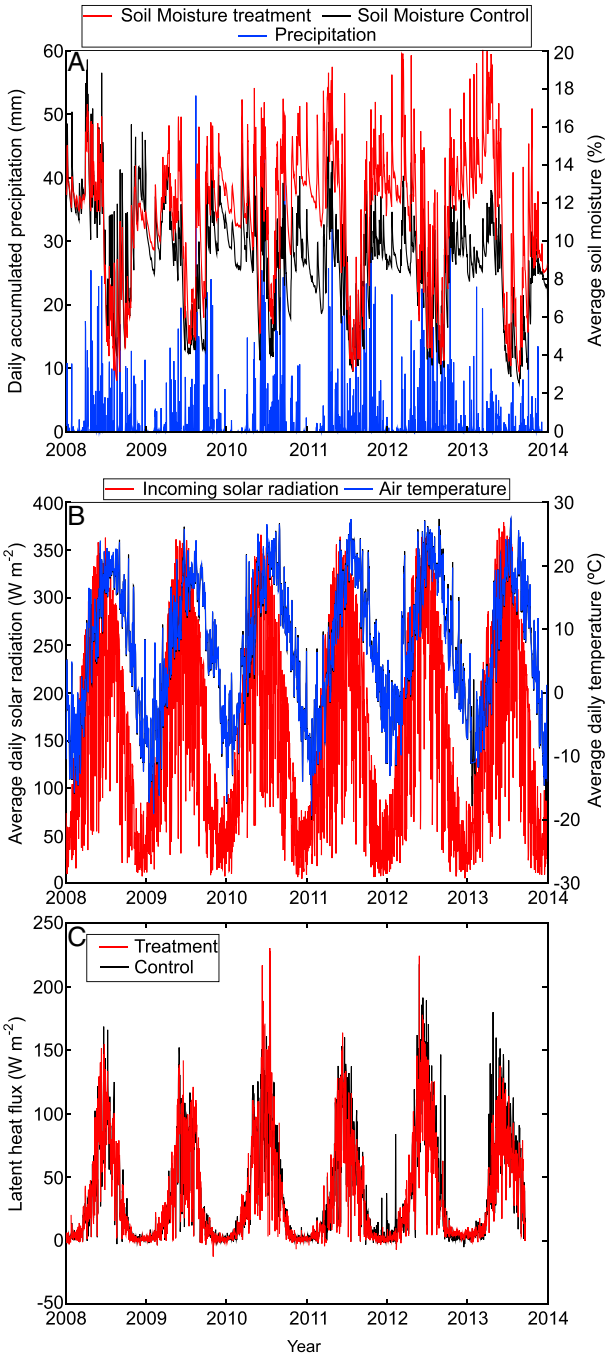

Figure 2. Time series of (a) daily total precipitation (mm) and daily mean soil moisture (%); (b) daily mean incoming solar radiation and temperature; and (c) daily mean latent heat flux, for the control and treatment plots from 2008 to 2014. Measurements in the treatment plot began in 2008, the same year the girdling took place, thought the girdling treatment took 1–2 years to take full effect and defoliate the girdled trees.

Though all the observations in both plots are ongoing and continuous year round, in this study we only analyzed data centered on the peak of the growing season. The length of each growing season was determined using the carbon-flux phenology approach [*Garrity et al.*, 2012] from observational net ecosystem exchange (NEE). Following *Matheny et al.* [2014], we further focused on the peak growing seasons by using observations during periods when C uptake flux was at least 40% of the annual peak of the 1 month moving average of NEE. This rather arbitrary threshold guarantees that we do not include days during the seasonal transition period in our analysis. In our plots, this peak growing season was days of year (DOY) 160–264, 144–250, and 153–262 for the years 2011–2013, respectively.

Due to the limited area of the treatment plot (39 ha), the footprint of the flux measurements occasionally included fluxes that originated outside of the disturbed plot. A 2-D footprint model [*Detto et al.*, 2006; *Morin et al.*, 2014] was used to approximate how much of the measured flux came from the disturbed plot on the basis of wind speed, direction, surface roughness height, and atmospheric boundary layer stability. Fluxes for the treatment plot were corrected assuming that the observed total flux for each half hour was a mixture of fluxes from a control-like forest (surrounding the treatment plot) and from the treatment plot itself. Using the footprint probability and the observed flux in the control plot, we determined the flux rate for the treatment plot as

$$\mathrm{LE}_f = \frac{\mathrm{LE}_m - (1 - F_p)\mathrm{LE}_c}{F_p} \quad (12)$$

Where LE_f is the corrected latent heat flux from the treatment plot, LE_m is the latent heat flux as measured from the US-UMd tower (which represents a mixture of mostly disturbance flux and some flux from the control-like surrounding forest), F_p is the spatially integrated footprint probability of the treatment plot, and LE_c is the latent heat flux measured at the same time in the control plot, which is representative of the

undisturbed forest surrounding the treatment plot. This correction rarely affected LE_f by more than 10% of LE_m.

2.9. Hysteresis

Sap flux, similar to transpiration, exhibits diurnal hysteresis that can be illustrated by plotting J_s as a function of VPD during the course of each day [*Chen et al*., 2011; *O'Grady et al*., 2008]. The plot traces a clockwise loop characteristic of the system's hysteresis [*Matheny et al*., 2014; *Novick et al*., 2014; *Verbeeck et al*., 2007a; *Zhang et al*., 2014]. In this work, the "hysteresis" of sap flux was expressed as the area encompassed by the loop. We restricted the definition of "day" in this calculation to include only daylight hours ($PAR > 100\ \mu mol\ m^{-2}\ s^{-1}$) and artificially closed the loop by connecting the first point of the day with the last to allow a closed-form integration. We analyzed both the relative hysteresis, where sap flux and VPD are normalized by their respective daily maxima and averaged among trees and days, and the absolute hysteresis where sap flux is not normalized.

2.10. Penman-Monteith Model

Periods when the soil water potential is low are typically also characterized by low humidity and high radiation (clear sky). Because air temperature, VPD, and soil moisture tend to be cross correlated, any direct correlation of evaporation with one of these variables would have confounded the interpretation of the effects of the others. To isolate the effects of soil water potential, we used the Penman-Monteith (PM) model [*Monteith*, 1965; *Penman*, 1948; *Thom*, 1972] to estimate the expected transpiration for each species/size bin during each half-hour observation period, given the atmospheric forcing (VPD, wind speed, humidity, and temperature) at that time and plot. The formulation we used does not include a term to incorporate the effects of soil moisture. We also used a general parameterization and did not include separate parameters for each species/size (equations (13) and (14)), thus assuming that transpiration per leaf area is constant across all species and sizes. The model predictions, therefore, represent the expected transpiration given the observed meteorological forcings (accurate within the model's goodness of fit) but do not include the effects of soil moisture or the differences between species/sizes. We fitted a PM transpiration model to the observed plot level latent heat flux and then tested the effects of soil moisture on the residual between the observed evapotranspiration and the model's predictions. We chose the PM model for this analysis as it is widely used and accepted for estimating LE, while it does not include any mechanistic link between soil water potential and stomatal conductance [*Ershadi et al*., 2014; *Stannard*, 1993]. The PM model predictions for transpiration, E_{PM} ($W\ m^{-2}$) therefore represent our null hypothesis to test for species/size, and soil moisture effects on transpiration.

$$E_{PM} = \frac{\Delta(R_n - G) + \frac{\rho C_p VPD}{r_h}}{\Delta + \frac{\gamma(r_c + r_h)}{r_h}} \tag{13}$$

where Δ is the slope of the saturation vapor pressure curve ($kPa\ K^{-1}$), ρ is the density of air ($g\ m^{-3}$), C_p is the specific heat of air ($J\ g^{-1}\ K^{-1}$), γ is the psychrometric constant as a function of air density and the heat capacity of air ($kPa\ K^{-1}$), r_h is the aerodynamic resistance to heat flux ($s\ m^{-1}$) following *Stannard* [1993], r_c is the stomatal resistance calculated from *Leuning* [1995]:

$$r_c = \frac{1}{g_0} + \frac{(C_s - \Gamma)\left(\frac{1+VPD}{D_0}\right)}{aA_C} \tag{14}$$

where C_s is CO_2 concentration in the air (ppm), Γ is the CO_2 compensation point in the absence of dark respiration (ppm) calculated following *Leuning et al*. [1995], and A_C is the CO_2 assimilation rate ($\mu mol\ m^{-2}\ s^{-1}$) calculated following *Leuning et al*. [1995]. The parameters for minimum leaf conductance, g_o ($mol\ m^{-2}\ s$), the reference vapor deficit, D_o (kPa), and a (a dimensionless shape parameter), were optimized using a Markov Chain Monte Carlo optimization algorithm with the sum of squared errors between daily integrated LE and E_{PM} minimized by the objective function [*Andrieu et al*., 2003]. The optimization of these parameters accounts for the scaling between leaf-scale resistance [*Leuning*, 1995] and canopy-scale resistance [*Thom*, 1972]. We use a species/size scaling factor, S_{sj}, to partition plot level E_{PM} into the fraction assumed to be contributed by each species/size bin ($E_{PM,sj}$) for comparison with species-specific transpiration (E_{sj}). In

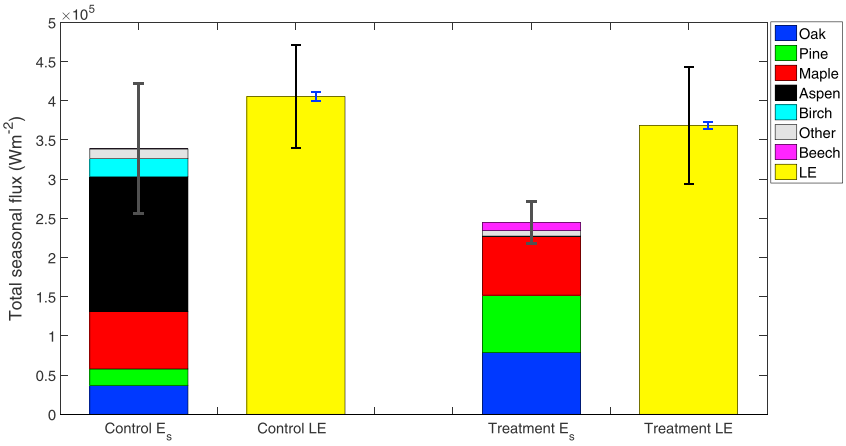

Figure 3. Total seasonal flux from each of the dominant species in each plot. The bar represents average values for the period of observation; the error bars on E_S represent the standard deviation of total plot E_C between years. The black error bar (left) on LE represents the standard deviation between years. The blue error bar (right) on LE represents the average annual closure deficit in the energy budget.

order to partition leaf area into size bins for each species test, we assumed that the leaf to sapwood area ratio is constant across sizes for each species.

$$E_{PM,sj} = E_{PM} S_{sj} \tag{15}$$

$$S_{sj} = \frac{\sum_k A_{sjk}}{\sum_j A_{sj}} \frac{A_{L,s}}{LAI} \tag{16}$$

where LAI is the plot total leaf area index.

2.11. Statistical Analysis

Statistical analysis was performed using JMP 11 (SAS Corporation, Cary, NC, USA). General linear models were used for both the PM-residual analysis and the hysteresis analysis of variance. Variables of year, plot, species, and size were common for both models. For the PM analysis, the effects of the four common variables and Ψ_{30cm} on the root-mean-squared error (RMSE) between E_{sj} and E_{PMsj} were tested. The hysteresis analysis tested the effects of the four common variables, daily mean *VPD*, daily mean PAR, and daily mean Ψ_{30cm} on the absolute hysteresis. For both models, year was assigned as a nominal variable with a random effect. Plot and species were also treated as nominal variables for both tests, and size was specified as ordinal according to the specified bins.

3. Results

The observed average seasonal LE at the control plot was 10.0% higher than that of the disturbed plot. Seasonal plot level canopy transpiration that was determined from sap flux measurements, E_C, in the control plot made up 76.3%, 93.3%, and 86.4% of plot level LE for 2011–2013, respectively. For the treatment plot, sap flux-driven total E_C constituted 66.9, 58.3, and 67.4% of LE. The deficit of the energy budget, δ, was used to estimate the confidence in LE measurements and was represented by the right most error bar on *LE* for each plot (1.4% and 1.3% for the control and treatment plots, respectively), Figure 3. The majority of transpiration (51.0%) in the control plot was supplied by bigtooth aspen trees, followed by red maple (21.4%). Transpiration at the treatment plot was dominated by red oak and red maple (33.1% and 31.1%, respectively) (Figure 3).

Although species differences in stand-level fluxes can be partially attributed to relative differences between control and treatment plots in terms of stand basal area of each species, notable differences in species' behaviors between treatments were apparent after normalization by the sapwood area of each species in each plot. Integrated daily J_s was 53.2% greater for red oaks in the treatment plot, as compared to the control plot (Figure 4). Conversely, red maples and white pines in the treatment plot show only slightly higher integrated daily sap flux density than those in the control plot by 6.1% and 5.7%, respectively (Figure 4).

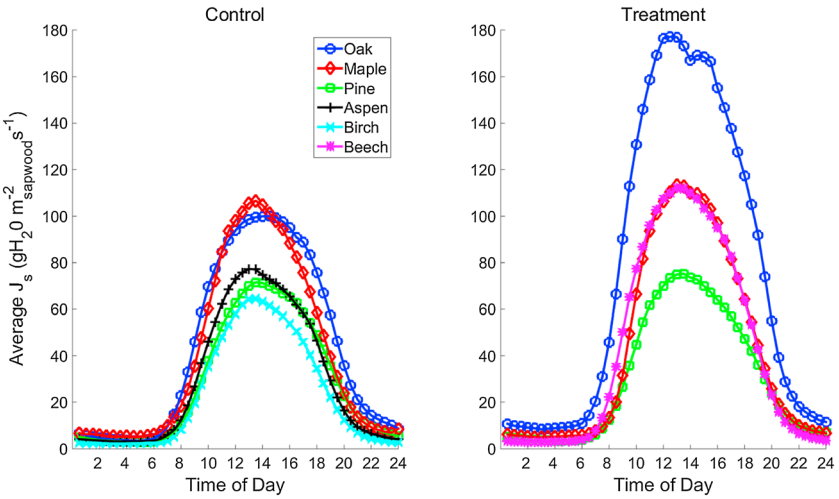

Figure 4. Mean seasonal diurnal sap flux density per sapwood area (J_s) ($gH_2O\ m^{-2}_{sapwood}\ s^{-1}$) at the (left) control plot and (right) treatment.

All species in both plots exhibited some degree of afternoon suppression of g_s (Figure 5). The most pronounced reductions occurred in bigtooth aspen (Figure 5d), red maple (Figures 5d and 5h), and white pine in the treatment plot (Figure 5h). Red oak demonstrated a moderate reduction of g_s near 3 pm but rebounded shortly after (Figure 5). Overall, red maple trees in the treatment plot showed a 29.5% greater reduction in total peak daily g_s than those in the control plot (Figures 5d and 5h). Conversely, red oak and white pine showed an increase in daily peak g_s in the treatment plot relative to the control plot (Figures 5d and 5h). The mean daily integrated g_s of red maple in the control plot exceeded that of maple in the treatment plot by 36.8%; while, red oak and white pine g_s in the treatment plot exceeded those in the control plot by 62.5 and 132.2%, respectively (Figures 5d and 5h). It is also clear from the size breakdown that small trees contribute a negligible portion of the evaporation per leaf area as compared to the contributions of canopy-dominant/codominant medium and large trees (Figure 5).

Stomatal conductance is not directly observed but calculated from observed sap flow (equations (9) and (10)). The calculation includes the observed values of air temperature, pressure, and *VPD*. To estimate the sensitivity of the calculated stomatal conductance, g_{sj}, to differences in microclimatic environmental

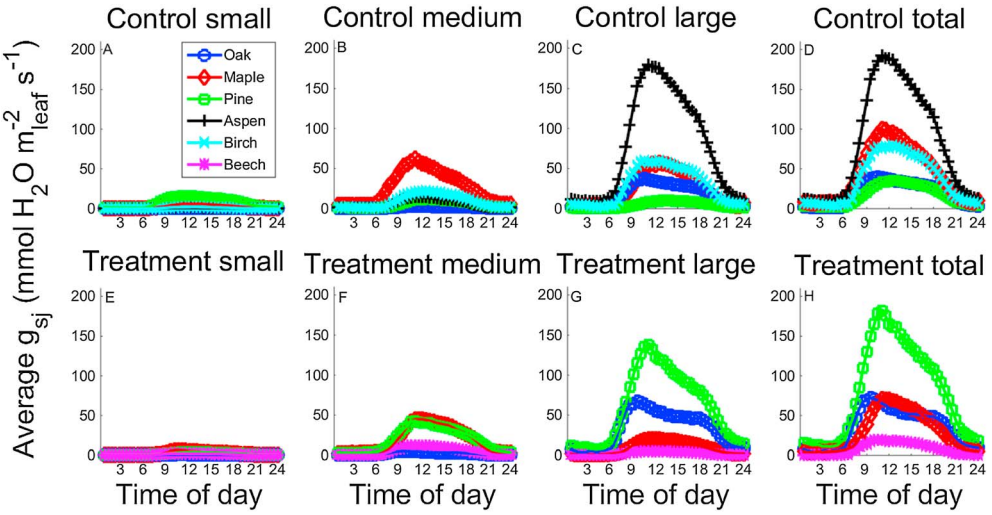

Figure 5. Average diurnal stomatal conductance over all seasons (g_{sj}) (mmol $H_2O\ m^{-2}_{leaf}\ s^{-1}$) by species/size class in the control and treatment plots. Total stomatal conductance refers to the sum of all size classes of trees of each species (g_s). Small trees (DBH < 10 cm), medium trees (10 cm ≤ DBH < 20 cm), large trees (DBH ≥ 20 cm).

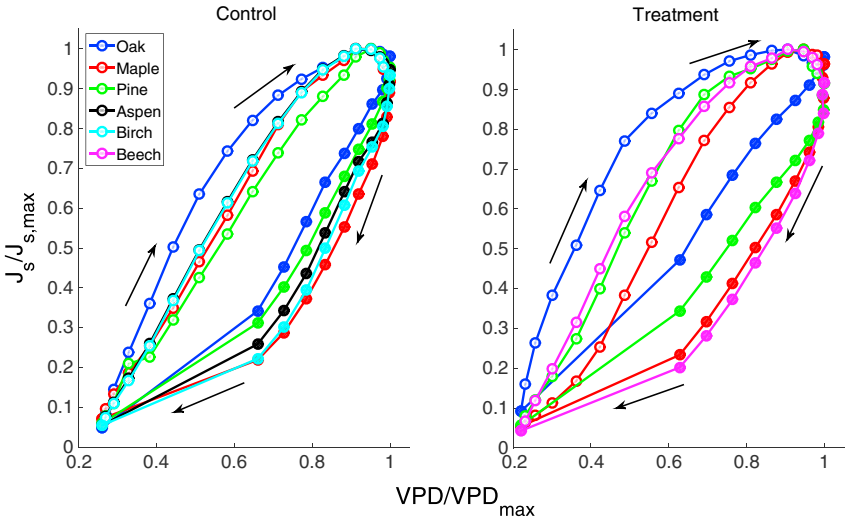

Figure 6. Relative hysteresis between sap flux and VPD during daylight hours over all size classifications for each species. Both J_s and VPD have been normalized by their respective daily maxima. Open symbols represent prenoon hours, closed symbols are afternoon. Arrows indicate the direction of the hysteresis.

conditions (air temperature, pressure, and VPD) between plots, we calculated g_{sj}' for each plot, combining the observed sap flux density from that plot with atmospheric forcing from the alternate plot. The mean daily root-mean-squared difference between g_{sj} and g_{sj}' was 17.0 and 6.7 mmol H_2O m_{leaf}^{-2} s^{-1} for the control and treatment plots, respectively. This indicates that differences in microclimatic conditions between the plots may account for up to 19.0% and 7.6% of the variation in each plot's mean stomatal conductance, for the control and treatment plots respectively.

In addition to changes in the external environmental drivers of stomatal conductance, we observed changes to relative C allocation to different pools within the tree after the disturbance treatment. In the 3 year period studied, white pines in the control plot and American beech in the treatment plot demonstrated the largest increases in basal area annually of all species (Table 3). Red oaks and red maples in the treatment plot both increased in basal area more quickly than the representative counterparts in the control plot (Table 3). Interestingly, red oaks are the sole species in the treatment plot to show a decline in LAI and leaf area per sapwood area over the three study years (Table 3). Although, in the control plot, red oaks, white pine, and paper birch showed similar declines in LAI and leaf area per sapwood areas (Table 3). White pines in the treatment plot and red maples in both plots gained in LAI and leaf area per sapwood area (Table 3). American beech in the treatment plot showed the largest annual increase in LAI and leaf per sapwood area ratios at 32.5% and 28.6%, respectively.

In both plots, stomatal conductance achieved its daily maxima between 11 A.M. and noon while sap flux density peaks between 1 and 2 P.M. (Figures 4 and 5). The difference between the morning and the afternoon response to the same or similar forcing conditions resulted in hysteresis between J_s and *VPD* (Figure 6). Red oak in the treatment plot and red maple in the control exhibited the largest absolute hysteresis, while white pine and paper birch tended to have the lowest hysteresis overall (Table 5). Typically, the largest absolute hysteresis occurred for all trees when VPD is high. A general linear model (overall $R^2 = 0.22$) showed significant effects of plot, species, tree diameter (size), Ψ_{30cm}, and VPD (Table 5) on absolute hysteresis. Ψ_{30cm} was found to have a significant interaction with tree size. The interaction between VPD and species was also significant (Table 5). PAR and VPD were also shown to have a significant combined effect, although the independent effect of PAR was not significant (Table 5). The total absolute hysteresis in different species under different dry-moist conditions is shown in Table 6, a complete breakdown by species/size category is provided in Table S1 in the supporting information.

Overall, intermediate disturbance in the treatment plot increased mean seasonal evaporative demand per total plot leaf area by 34% as compared to the control plot (Tables 1 and 3). However, compensatory growth

Table 5. Absolute Hysteresis Analysis Statistics Using a Simple Linear Model ($R^2 = 0.22$)

Variable	*F* Ratio	*P* value	Partial R^2
Plot	10.53	0.0012	8.13E-04
Species	195.08	<0.0001	8.38E-02
Size	62.26	<0.0001	2.25E-02
VPD	13.78	0.0002	8.80E-05
PAR	0.31	0.5753	1.74E-03
Ψ_{30cm}	57.15	<0.0001	4.41E-02
Species × Plot	9.52	<0.0001	2.14E-02
Ψ_{30cm} × Species	0.31	0.7337	1.16E-04
Ψ_{30cm} × Size	41.50	<0.0001	1.40E-02
VPD × Species	31.87	<0.0001	1.08E-02
VPD × Size	1.11	0.3281	3.81E-04
VPD × PAR	115.93	<0.0001	1.98E-02

in terms of increases in basal area and therefore sapwood area, helped to overcome the increased demands (Table 4). There were significant differences between plots in a particular species' absolute hysteresis (Table 5). The effect of plot on absolute hysteresis over all species was significant, as were the effects of Ψ_{30cm} and VPD (Table 5). This indicates that differences between plots exist outside of the influence of Ψ_{30cm} and VPD. The combined effect of soil water potential and size was stronger for smaller trees (DBH < 20 cm, $P < 0.0001$) than it was for larger trees (DBH ≥ 20 cm, $P = 0.0068$). VPD was shown to have a significant combined effect with species, but not with tree size.

To test the independent effect of soil water potential on sap flux regardless of air temperature and humidity, we compared E_{sj} from each species/size bin with the PM modeled value, $E_{PM,sj}$. The root-mean-square half-hourly error (RMSE) between the observed values and the model represented the portion of the variation in E_{sj} that was not explained by VPD, light levels, wind speed, and air temperature, whose effects are included in the PM model with the *Leuning* [1995] stomatal conductance parameterization. Species, size, plot, and Ψ_{30cm} had significant effects on transpiration (Table 7). Here we distinguish the direct effects of Ψ_{30cm} on transpiration from the effects of the other plot-specific forcings (light, wind, VPD, temperature, LAI), which are accounted for by the PM model. Interactions between Ψ_{30cm} and species and Ψ_{30cm} and size were also significant (Table 7). These effects were found to account for some, but not all of the model RMSE between E_{sj} and $E_{PM,sj}$ ($R^2 = 0.40$). When analyzed with respect to Ψ_{30cm} alone, the PM model was found to have lower RMSE during well-watered conditions than when water was limiting, as was expected ($R^2 = 0.04$, $P < 0.0001$, slope $= -0.62$).

4. Discussion

Transpiration in the disturbed treatment plot was reduced when compared to that of the control plot. On average, our sap flux measurements accounted for 85.6% of LE in the control plot and 64.2% in the treatment

Table 6. Average Absolute Hysteresis (g $m^{-2}_{sapwood}$ s^{-1}) for Each Species' J_s Over All Days, Days With Wet, Intermediate, and Dry Soil, and Days With Low, Intermediate, and High VPD for Both Plots. Plot Total Hysteresis is the Hysteresis of J_C. Values Listed as ± are Standard Deviation Among Days Having Each Environmental Condition (e.g., Wet Soil, High VPD)

	Red Oak	White Pine	Red Maple	Bigtooth Aspen	Paper Birch	Plot Total
			Control			
All conditions	20.2 ± 25.9	10.7 ± 11.7	24.3 ± 21.0	18.5 ± 16.8	15.0 ± 9.7	108.2 ± 84.2
Wet soil	16.2 ± 26.0	8.4 ± 11.3	18.6 ± 20.4	14.7 ± 16.7	8.5 ± 10.6	84.6 ± 84.8
Low *VPD*	17.0 ± 17.7	6.5 ± 11.6	13.6 ± 16.9	11.0 ± 14.5	10.6 ± 9.3	68.9 ± 77.5
Int. soil	13.6 ± 16.6	8.3 ± 11.6	21.1 ± 25.3	14.2 ± 17.7	5.1 ± 9.0	86.2 ± 101.1
Int. *VPD*	21.8 ± 31.0	12.6 ± 11.4	28.9 ± 20.2	21.5 ± 16.1	18.0 ± 8.7	124.8 ± 79.7
Dry soil	6.9 ± 11.1	2.6 ± 5.6	8.9 ± 12.7	4.7 ± 7.4	4.5 ± 7.7	37.4 ± 52.7
High *VPD*	22.6 ± 10.7	14.4 ± 9.3	37.3 ±23.0	28.8 ± 19.1	20.3 ± 10.5	155.0 ± 81.5
			Treatment			
	Red Oak	White Pine	Red Maple	American Beech	Plot Total	
All conditions	31.4 ± 28.4	12.2 ± 10.3	20.6 ± 18.5	21.5 ± 18.7	94.2 ± 68.4	
Wet soil	26.0 ± 29.9	10.7 ± 11.0	16.6 ± 18.6	17.3 ± 18.9	76.5 ± 72.0	
Low *VPD*	27.8 ± 33.1	8.2 ± 11.6	9.2 ± 17.5	9.9 ± 17.7	68.1 ± 82.1	
Int. soil	21.6 ± 26.6	7.8 ± 9.6	13.9 ± 17.6	14.5 ± 18.1	65.8 ± 72.1	
Int. *VPD*	33.4 ± 26.9	14.2 ± 9.4	24.7 ± 16.4	25.7 ± 16.6	105.0 ± 58.8	
Dry soil	19.1 ± 22.9	5.8 ± 7.7	14.3 ± 18.8	15.1 ± 19.4	60.9 ± 71.9	
High *VPD*	31.7 ± 21.8	12.9 ± 8.2	29.8 ± 17.2	30.9 ± 17.2		

Table 7. Penman-Moneith Residual Analysis Statistics Using a Simple Linear Model ($R^2 = 0.40$)

Variable	*F* Ratio	*P* value	Partial R^2
Plot	24.44	<0.0001	2.21E-02
Species	203.30	<0.0001	1.18E-01
Size	78.23	<0.0001	9.88E-03
Ψ_{30cm}	26.92	<0.0001	2.00E-06
$\Psi_{30cm} \times$ Species	994.87	<0.0001	2.60E-01
$\Psi_{30cm} \times$ Size	39.49	<0.0001	2.03E-02

plot. Discrepancies between E_C and LE at each plot are primarily due to sources of evaporation that were accounted for in LE but were not included in sap flow measurements, such as soil evaporation, transpiration from understory vegetation and from trees smaller than 8 cm in diameter, and evaporation of intercepted precipitation from and condensation on leaf surfaces. It is most likely that the larger discrepancy between E_C and LE in the treatment plot was related to increased understory transpiration, due to increased light penetration through the more open canopy that characterizes the disturbed plot [*Hardiman et al*., 2013]. In their study of soil moisture in these same plots, *He et al*. [2013] similarly found *ET* to be lower in the treatment plot, but that enhanced soil evaporation was not sufficient to completely offset the difference in total LE. Between the two plots, there were relatively small differences in atmospheric conditions (*VPD*, temperature, and pressure) such that, in accordance with our g_{sj}-g_{sj}' analysis, ~7–19% of the differences in water flux between plots could be attributed to the differences in forcing. *He et al*. [2013] found that canopy interception typically accounted for ~11–25% and up to 31% of precipitation in our plots with reduced interception in the disturbance plot. It is unlikely that the lower treatment plot E_C could be the outcome of biased species representation among the instrumented trees. Only 2% of stand basal area in the treatment plot is made up of species that were not represented by our sap flux study. It is equally unlikely that E_C/LE mismatch is due to errors in measured LE. Errors in the energy balance were found to be very small (1.4% and 1.3% for the control and treatment plots, respectively), indicating high accuracy of eddy covariance measurements.

Although transpiration accounting for ~80% of LE in dry sites is not unheard of [*Miller et al*., 2010], we acknowledge that our lack of sap flux measurements over depth ranges within the sapwood and radial scaling of sap flux measurements contributed to errors in the sap flux data [*Phillips et al*., 1996; *Schäfer et al*., 2000]. Due to the increased number of large red maples and large bigtooth aspen trees in the control plot, these errors were likely greater in the control plot and would reduce the fraction of LE that is accounted for by E_C in that plot. Using a rough estimate, we computed the percentage of sapwood area that is beyond the reach of the 20 mm probes and assumed a 50% reduction of J_s in this inner sapwood area. On this basis, we expected an overestimation of E_C of roughly 11% in the control plot and 3.7% in the treatment plot. Due to the dependence of radial patterns in sap flow on species, tree age, and site history and, therefore, the large variability among reduction factors, we chose to disclose this limitation rather than to assume the applicability of a reduction factor from existing literature that was not specific to our plots [*James et al*., 2002; *Nadezhdina et al*., 2002; *Phillips et al*., 1996; *Renninger et al*., 2013; *Schäfer et al*., 2000; *Shinohara et al*., 2013]. Despite these errors, the roughly 15% difference in transpiration between the control and treatment plots remains significant.

It has been suggested that transpiration at a landscape scale must be invariant because there is a finite amount of incoming radiation to a square meter of land [*Enquist*, 2002]. Nonetheless, it is important to note that such scaling laws refer to vegetation that has established an "optimized," steady state canopy. The intermediate disturbance in our treatment plot served to disrupt any preexisting optimization the canopy may have achieved. This disturbance led to a period of rapid transition characterized by changes to nitrogen [*Nave et al*., 2011], carbon [*Gough et al*., 2013], and light penetration [*Hardiman et al*., 2013]. It has also been shown through multiple studies that plants having diverse functional traits (isohydric/anisohydric, ring/diffuse porous, and broadleaf/conifer) scale transpiration with environmental forcings in a nonlinear and unique manner [e.g., *Baldocchi*, 2005; *McCulloh et al*., 2012; *Wullschleger et al*., 2001]. These differences in forcings and species/size composition combine with specific functional traits of the species in our plot to produce a plot level water flux that is significantly altered from that of the undisturbed control plot.

Of the three species compared between plots, each presented a different hydraulic functional type and showed a unique response to the changed forcing conditions due to the disturbance treatment, thus supporting our hypothesis that the capacity to increase transpiration following intermediate disturbances would differ between trees with opposing hydraulic strategies. Red maples, diffuse porous and relatively isohydric, showed

lower transpiration per leaf area and lower stomatal conductance in the treatment plot than in the control plot. This was in contrast to red oaks, ring porous and relatively anisohydric, that showed higher sap flux density, transpiration per leaf area, and stomatal conductance in the treatment plot than those in the control plot. White pines, a conifer, showed a small increase in sap flux density in the disturbance area while their transpiration per leaf area and stomatal conductance increased. Differential growth may account for a portion of these differences. Maples at the treatment plot had more leaf area per xylem area than those in the control plot, while oaks and pines in the treatment plot had fewer leaves per xylem area. On average, basal area for oaks and maples increased more quickly in the treatment plot than in the control, whereas pines in the treatment plot showed lower average annual basal growth rate than those in the control plot.

Interestingly, red maple was the only species for which the effect of plot on absolute hysteresis was significant ($P = 0.0003$). Red maple was also the sole species in the control plot, where medium-sized codominant trees exhibited stomatal conductance at similar levels to dominant trees of that species, and in the treatment plot the codominant medium-sized individuals showed higher conductance than the canopy-dominant maples (Figure 5). The performance of the larger canopy-dominant maples might indicate that maples are more sensitive to photoinhibition or thermal injury and tend to be more productive in partially shaded situations [*Aber et al*., 1982; *Pastor et al*., 1982]. This finding is consistent with the work of *Kitao et al*. [2006] who found that a shade acclimated species of maple was more susceptible to photoinhibition after gap formation than a similarly acclimated species of oak. Additionally, it was shown by *Webster and Lorimer* [2003] that shade intolerant species tend to be more efficient in terms of bole growth to projected crown area growth. This finding is supported by our observations of more rapid bole growth by the moderately shade intolerant red oaks [*Chapman and Gower*, 1991] than in more tolerant red maples [*Aber et al*., 1982; *Webster and Lorimer*, 2003] in both study plots.

We used the hysteretic relationship between sap flux and VPD to quantify changes in plant water status throughout the day. This response has been previously linked to soil moisture, VPD, and plant physiology [*Matheny et al*., 2014; *Novick et al*., 2014; *Unsworth et al*., 2004; *Verbeeck et al*., 2007b; *Zhang et al*., 2014]. Red oaks had the largest mean absolute hysteresis in the treatment plot, the second largest mean absolute hysteresis in the control plot, and the largest mean relative hysteresis in both plots. This finding upholds our third hypothesis that anisohydric species would demonstrate larger hysteresis and hydraulic stress. Red oaks have a smaller number of large-diameter vessels and operate on the efficiency end of the "safety-efficiency" continuum [*Manzoni et al*., 2013]. Therefore, these trees required more time to replenish greater amounts of lost xylem water and to refill embolized vessels after depleting initial capacitance which lead to lower sap flux in the afternoon as compared to more isohydric species such as maple [*McCulloh et al*., 2012; *Taneda and Sperry*, 2008; *Tyree and Zimmermann*, 2002]. Bigtooth aspen and paper birch, on the opposing safety end of the "safety-efficiency" continuum tended to exhibit smaller degrees of hysteresis, with the exception during days when VPD was very high. Isohydric trees, such as maples, regulate their stomatal conductance to keep leaf water potential relatively constant throughout the day [*Thomsen et al*., 2013], as evidenced by the larger decline in afternoon stomatal conductance we found in red maple relative to red oak. Surprisingly, red maples exhibited the largest mean absolute hysteresis in the control plot. It is possible, and consistent with the finding of *Thomsen et al*. [2013], that the larger absolute hysteresis in red maples in the control plot was related to the species' sensitivity to soil water potential and the relatively drier conditions in that plot. Additionally, when compared on the basis of relative hysteresis, when sap flux has been normalized by the maximal sap flux for that day, red maples in both plots demonstrated lower relative hysteresis than shown by red oaks. White pine, the only coniferous species in this study, consistently had the least amount of diurnal hysteresis, which is consistent with the results of *McAdam and Brodribb* [2014] and *Matheny et al*. [2014] for other conifers. These different responses to soil water availability and canopy light penetration discussed above support the first half of our second hypothesis, that disturbance-related changes to external physical drivers of transpiration would influence the diurnal pattern of transpiration more strongly in some species than others. However, the larger hysteresis presented by the control plot red maples relative to those the treatment plot refuted our prediction that the isohydric species, red maple, would show more hydraulic stress in the postdisturbance microclimate.

The diurnal hysteresis of transpiration as a means to quantify hydrodynamic limitation is limited by the combination of factors that control its magnitude. As described by *Zhang et al*. [2014], the hysteretic nature of transpiration is partially due to the depletion of internal plant water throughout the day but is also driven in

part by the time lag between VPD and PAR. Hysteresis is further complicated by the influence of both short-term (half-hourly) dynamics of fast processes, such as stomatal conductance [*Unsworth et al*., 2004], and longer-term dynamics (days-weeks) of slower processes such as soil drought [*Wullschleger et al*., 1992]. Hysteresis will consistently be larger on days when peak transpiration is high. Normalizing the components of hysteresis, transpiration, and VPD, by their respective daily maxima helped to reduce this effect. However, because hysteresis is defined as the area encompassed by the loop, this form of linear normalization was only partially effective to eliminate this bias for days when transpiration was large. Conversely, during days when soil water potential was very low (i.e., dry soil conditions), hysteresis was minimal if transpiration was low throughout the entire day, because both morning and afternoon transpiration were close to zero. Therefore, hydraulic stress should not be evaluated on the basis of hysteresis alone, but as a combination of hysteresis with the skewness of the daily patterns of sap flux and stomatal conductance, and the total transpiration per leaf and sapwood area.

Our comparative analysis of the PM-simulated transpiration showed that discrepancies between expected transpiration and sap flux arose from differences between species and size distributions, which could not be accounted for by linear scaling of sapwood area and leaf area alone. This may be particularly true following intermediate disturbance, which results in diversification of tree structural dimensions [*Hardiman et al*., 2013]. This finding supported our fourth hypothesis, that predisturbance and postdisturbance transpiration are distinct in such a manner that adjustment on the basis of LAI alone is not sufficient to adequately represent disturbance in land surface models. Additionally, the PM model residual analysis demonstrated significant interactions of soil water potential with species and size, and analysis of hysteresis revealed significant interactions between soil water potential and tree size indicating that improving the representation of the mechanisms by which soil moisture affects stomatal conductance, and species or hydraulic functional-type parameterization could improve model performance [*Bohrer et al*., 2005; *Grant et al*., 2006; *Janott et al*., 2011; *Weng and Luo*, 2008]. There was a significant decline in transpiration postdisturbance, beyond the extent that is predicted by the differences in atmospheric forcings and LAI, and the hysteresis analysis revealed important differences between species behavior in disturbed and undisturbed plots.

5. Conclusion

Intermediate disturbance impacted plot level transpiration through changes to the external physical drivers including mean wind speed, turbulent mixing, air temperature, humidity, canopy structure and light penetration, and soil water conditions. Long-term, half-hourly records of sap flux and stomatal conductance revealed species/size-specific responses to disturbance. We found that the differences in transpiration between species and between disturbed/undisturbed plots were significant even after the differences in external environmental forcing were accounted for using the Penman-Monteith model, and even when adjusted for the effects of disturbance-induced changes to leaf-to-sapwood area ratio. These nongeneralizable differences in species response to disturbance in terms of where C is allocated (i.e., xylem or leaves) and water flux have important implications for land surface modeling [*Schäfer et al*., 2014]. Frequently, red oaks and red maples are coclassified in ecosystem models as the same plant functional type (temperate, midsuccessional, and deciduous). However, our results, along with those highlighting the differences between the hydraulic functional types [*Thomsen et al*., 2013], showed that these species behave distinctly from one another and respond differently to changes in forest structure. Similar to *Ewers et al*. [2008] who found three different values for daily E_L for sugar maple in three different plots, we found that daily sap flow per sapwood area, stomatal conductance, and transpiration per leaf area will change depending on a site's history and the disturbance regimen.

A combined analysis using hysteresis and sap flux with soil water status demonstrated changes in plant hydraulic status consistent with the behaviors of isohydric and anisohydric strategies. Understanding the mechanisms that shape plot level transpiration and how they influence forests' response to disturbance will help modelers eliminate errors and better capture changes to water and C fluxes as forests are shaped by natural succession and other disturbances, as well as climate and land-use change. The incorporation of advanced hydrodynamic models for hydraulic functional-type-specific stomatal parameterization (e.g., Finite Elements Tree-Crown Hydrodynamic model (FETCH) [*Bohrer et al*., 2005] or Expert-N [*Janott et al*., 2011]) could help resolve these differences and improve the quality of simulated ET by land surface models, in general, and particularly in forests undergoing intermediate disturbance.

Acknowledgments

This research was supported by the U.S. Department of Energy's Office of Science, Office of Biological and Environmental Research, Terrestrial Ecosystem Sciences program under award DE-SC0007041 and DE-SC0006708, and the Ameriflux Management project under Flux Core Site agreement 7096915 through Lawrence Berkeley National Laboratory, the National Science Foundation grant DEB-0911461 including an REU supplement award for AMM, and a summer graduate student research grants by the University of Michigan Biological Station to AMM and THM. Additional support for the UMBS flux site was provided by the National Oceanic and Atmospheric Administration award NA11OAR4310190. Any opinions, findings, and conclusions or recommendations expressed in this material are those of the authors and do not necessarily reflect the views of funding agencies. The data for this paper are available by contacting the corresponding author.

References

Aber, J. D., J. Pastor, and J. M. Melillo (1982), Changes in forest canopy structure along a site quality gradient in southern Wisconsin, *Am. Midl. Nat.*, *108*(2), 256–265, doi:10.2307/2425486.

Allen, C. D., et al. (2010), A global overview of drought and heat-induced tree mortality reveals emerging climate change risks for forests, *For. Ecol. Manage.*, *259*, 660–684, doi:10.1016/j.foreco.2009.09.001.

Andrieu, C., N. de Freitas, A. Doucet, and M. Jordan (2003), An introduction to MCMC for machine learning, *Mach. Learn.*, *50*(1-2), 5–43, doi:10.1023/A:1020281327116.

Asase, A., B. K. Asiatokor, and K. Ofori-Frimpong (2014), Effects of selective logging on tree diversity and some soil characteristics in a tropical forest in southwest Ghana, *J. For. Res.*, *25*, 171–176, doi:10.1007/s11676-014-0443-4.

Asner, G. P., M. Keller, R. Pereira, J. C. Zweede, and J. N. M. Silva (2004), Canopy damage and recovery after selective logging in Amazonia: Field and satellite studies, *Ecol. Appl.*, *14*, S280–S298.

Baldocchi, D. D. (2005), The role of biodiversity on the evaporation of forests, in *Forest Diversity and Function: Temperate and Boreal Systems*, edited by M. SchererLorenzen, C. Korner, and E. D. Schulze, pp. 131–148, Springer, Berlin.

Bohrer, G., H. Mourad, T. A. Laursen, D. Drewry, R. Avissar, D. Poggi, R. Oren, and G. G. Katul (2005), Finite element tree crown hydrodynamics model (FETCH) using porous media flow within branching elements: A new representation of tree hydrodynamics, *Water Resour. Res.*, *41*, W11404, doi:10.1029/2005WR004181.

Bohrer, G., G. G. Katul, R. L. Walko, and R. Avissar (2009), Exploring the effects of microscale structural heterogeneity of forest canopies using large-eddy simulations, *Boundary Layer Meteorol.*, *132*, 351–382, doi:10.1007/s10546-009-9404-4.

Bovard, B. D., P. S. Curtis, C. S. Vogel, H.-B. Su, and H. P. Schmid (2005), Environmental controls on sap flow in a northern hardwood forest, *Tree Physiol.*, *25*, 31–38.

Chapin, F. S. (2003), Effects of plant traits on ecosystem and regional processes: A conceptual framework for predicting the consequences of global change, *Ann. Bot.*, *91*(4), 455–463, doi:10.1093/aob/mcg041.

Chapman, J. W., and S. T. Gower (1991), Aboveground production and canopy dynamics in sugar maple and red oak trees in southwestern Wisconsin, *Can. J. For. Res.*, *21*(10), 1533–1543, doi:10.1139/x91-214.

Chen, L. X., Z. Q. Zhang, Z. D. Li, J. W. Tang, P. Caldwell, and W. J. Zhang (2011), Biophysical control of whole tree transpiration under an urban environment in Northern China, *J. Hydrol.*, *402*, 388–400, doi:10.1016/j.jhydrol.2011.03.034.

Choat, B., et al. (2012), Global convergence in the vulnerability of forests to drought, *Nature*, *491*, 752–756, doi:10.1038/nature11688.

Clearwater, M. J., F. C. Meinzer, J. L. Andrade, G. Goldstein, and N. M. Holbrook (1999), Potential errors in measurement of nonuniform sap flow using heat dissipation probes, *Tree Physiol.*, *19*(10), 681–687.

Damour, G., T. Simonneau, H. Cochard, and L. Urban (2010), An overview of models of stomatal conductance at the leaf level, *Plant Cell Environ.*, *33*, 1419–1438, doi:10.1111/j.1365-3040.2010.02181.x.

Detto, M., and G. G. Katul (2007), Simplified expressions for adjusting higher-order turbulent statistics obtained from open path gas analyzers, *Boundary Layer Meteorol.*, *122*, 205–216, doi:10.1007/s10546-006-9105-1.

Detto, M., N. Montaldo, J. D. Albertson, M. Mancini, and G. Katul (2006), Soil moisture and vegetation controls on evapotranspiration in a heterogeneous Mediterranean ecosystem on Sardinia, Italy, *Water Resour. Res.*, *42*, W08419, doi:10.1029/2005WR004693.

Dietze, M. C., M. S. Wolosin, and J. S. Clark (2008), Capturing diversity and interspecific variability in allometries: A hierarchical approach, *For. Ecol. Manage.*, *256*, 1939–1948, doi:10.1016/j.foreco.2008.07.034.

Enquist, B. J. (2002), Universal scaling in tree and vascular plant allometry: Toward a general quantitative theory linking plant form and function from cells to ecosystems, *Tree Physiol.*, *22*(15-16), 1045–1064.

Ershadi, A., M. F. McCabe, J. P. Evans, N. W. Chaney, and E. F. Wood (2014), Multi-site evaluation of terrestrial evaporation models using FLUXNET data, *Agric. For. Meteorol.*, *187*, 46–61, doi:10.1016/j.agrformet.2013.11.008.

Ewers, B. E., and R. Oren (2000), Analyses of assumptions and errors in the calculation of stomatal conductance from sap flux measurements, *Tree Physiol.*, *20*(9), 579–589.

Ewers, B. E., D. S. Mackay, J. Tang, P. V. Bolstad, and S. Samanta (2008), Intercomparison of sugar maple (*Acer saccharum Marsh.*) stand transpiration responses to environmental conditions from the Western Great Lakes Region of the United States, *Agric. For. Meteorol.*, *148*, 231–246, doi:10.1016/j.agrformet.2007.08.003.

Fatichi, S., and V. Y. Ivanov (2014), Interannual variability of evapotranspiration and vegetation productivity, *Water Resour. Res.*, *50*, 3275–3294, doi:10.1002/2013wr015044.

Finnigan, J. J. (2004), A re-evaluation of long-term flux measurement techniques. Part II: Coordinate systems, *Boundary Layer Meteorol.*, *113*, 1–41, doi:10.1023/b:boun.0000037348.64252.45.

Fisher, J. B., T. A. DeBiase, Y. Qi, M. Xu, and A. H. Goldstein (2005), Evapotranspiration models compared on a Sierra Nevada forest ecosystem, *Environ. Modell. Softw.*, *20*, 783–796, doi:10.1016/j.envsoft.2004.04.009.

Ford, C. R., R. M. Hubbard, B. D. Kloeppel, and J. M. Vose (2007), A comparison of sap flux-based evapotranspiration estimates with catchment-scale water balance, *Agric. For. Meteorol.*, *145*, 176–185, doi:10.1016/j.agrformet.2007.04.010.

Ford, C. R., R. M. Hubbard, and J. M. Vose (2011), Quantifying structural and physiological controls on variation in canopy transpiration among planted pine and hardwood species in the southern Appalachians, *Ecohydrology*, *4*, 183–195, doi:10.1002/eco.136.

Forrester, J. A., D. J. Mladenoff, S. T. Gower, and J. L. Stoffel (2012), Interactions of temperature and moisture with respiration from coarse woody debris in experimental forest canopy gaps, *For. Ecol. Manage.*, *265*, 124–132, doi:10.1016/j.foreco.2011.10.038.

Garrity, S. R., K. Meyer, K. D. Maurer, B. Hardiman, and G. Bohrer (2012), Estimating plot-level tree structure in a deciduous forest by combining allometric equations, spatial wavelet analysis and airborne LiDAR, *Remote Sens Lett.*, *3*, 443–451, doi:10.1080/01431161.2011.618814.

Gough, C. M., C. S. Vogel, H. P. Schmid, H. B. Su, and P. S. Curtis (2008), Multi-year convergence of biometric and meteorological estimates of forest carbon storage, *Agric. For. Meteorol.*, *148*, 158–170, doi:10.1016/j.agrformet.2007.08.004.

Gough, C. M., C. S. Vogel, B. Hardiman, and P. S. Curtis (2010), Wood net primary production resilience in an unmanaged forest transitioning from early to middle succession, *For. Ecol. Manage.*, *260*, 36–41, doi:10.1016/j.foreco.2010.03.027.

Gough, C. M., B. S. Hardiman, L. E. Nave, G. Bohrer, K. D. Maurer, C. S. Vogel, K. J. Nadelhoffer, and P. S. Curtis (2013), Sustained carbon uptake and storage following moderate disturbance in a Great Lakes forest, *Ecol. Appl.*, *23*, 1202–1215, doi:10.1890/12-1554.1.

Granier, A. (1987), Evaluation of transpiration in a Douglas-Fir stand by means of sap flow measurements, *Tree Physiol.*, *3*(4), 309–319.

Grant, R. F., et al. (2006), Intercomparison of techniques to model water stress effects on CO_2 and energy exchange in temperate and boreal deciduous forests, *Ecol. Modell.*, *196*, 289–312, doi:10.1016/j.ecolmodel.2006.02.015.

Hardiman, B. S., G. Bohrer, C. M. Gough, and P. S. Curtis (2013), Canopy structural changes following widespread mortality of canopy dominant trees, *Forests*, *4*, 537–552, doi:10.3390/f4030537.

He, L. L., V. Y. Ivanov, G. Bohrer, J. E. Thomsen, C. S. Vogel, and M. Moghaddam (2013), Temporal dynamics of soil moisture in a northern temperate mixed successional forest after a prescribed intermediate disturbance, *Agric. For. Meteorol.*, *180*, 22–33, doi:10.1016/j.agrformet.2013.04.014.

Herms, D. A., and D. G. McCullough (2014), Emerald ash borer invasion of North America: History, biology, ecology, impacts, and management, in *Annual Review of Entomology*, edited by M. R. Berenbaum, pp. 13–30, Annual Reviews, Palo Alto, Calif.

Huang, C. Y., and W. R. L. Anderegg (2012), Large drought-induced aboveground live biomass losses in southern Rocky Mountain aspen forests, *Global Change Biol.*, *18*, 1016–1027, doi:10.1111/j.1365-2486.2011.02592.x.

James, S. A., M. J. Clearwater, F. C. Meinzer, and G. Goldstein (2002), Heat dissipation sensors of variable length for the measurement of sap flow in trees with deep sapwood, *Tree Physiol.*, *22*(4), 277–283.

Janott, M., S. Gayler, A. Gessler, M. Javaux, C. Klier, and E. Priesack (2011), A one-dimensional model of water flow in soil-plant systems based on plant architecture, *Plant Soil*, *341*, 233–256, doi:10.1007/s11104-010-0639-0.

Jasechko, S., Z. D. Sharp, J. J. Gibson, S. J. Birks, Y. Yi, and P. J. Fawcett (2013), Terrestrial water fluxes dominated by transpiration, *Nature*, *496*, 347–350, doi:10.1038/nature11983.

Kaimal, J. C., and J. E. Gaynor (1991), Another look at sonic thermometry, *Agric. For. Meteorol.*, *56*(4), 401–410, doi:10.1007/BF00119215.

Katul, G. G., R. Oren, S. Manzoni, C. Higgins, and M. B. Parlange (2012), Evapotranspiration: A process driving mass transport and energy exchange in the soil-plant-atmosphere-climate system, *Rev. Geophys.*, *50*, RG3002, doi:10.1029/2011RG000366.

Kitao, M., T. T. Lei, T. Koike, H. Tobita, and Y. Maruyama (2006), Tradeoff between shade adaptation and mitigation of photoinhibition in leaves of *Quercus mongolica* and *Acer mono* acclimated to deep shade, *Tree Physiol.*, *26*, 441–448.

Kucharik, C. J., J. A. Foley, C. Delire, V. A. Fisher, M. T. Coe, J. D. Lenters, C. Young-Molling, N. Ramankutty, J. M. Norman, and S. T. Gower (2000), Testing the performance of a dynamic global ecosystem model: Water balance, carbon balance, and vegetation structure, *Global Biogeochem. Cycles*, *14*(3), 795–825, doi:10.1029/1999GB001138.

Leuning, R. (1995), A critical appraisal of a combined stomatal-photosynthesis model for C3 plants, *Plant Cell Environ.*, *18*(4), 339–355.

Leuning, R., F. M. Kelliher, D. G. G. Depury, and E. D. Schulze (1995), Leaf nitrogen, photosynthesis, conductance and transpiration—Scaling from leaves to canopies, *Plant Cell Environ.*, *18*(10), 1183–1200, doi:10.1111/j.1365-3040.1995.tb00628.x.

Liebethal, C., B. Huwe, and T. Foken (2005), Sensitivity analysis for two ground heat flux calculation approaches, *Agric. For. Meteorol.*, *132*, 253–262, doi:10.1016/j.agrformet.2005.08.001.

Manzoni, S., G. Vico, G. Katul, S. Palmroth, R. B. Jackson, and A. Porporato (2013), Hydraulic limits on maximum plant transpiration and the emergence of the safety-efficiency trade-off, *New Phytol.*, *198*, 169–178, doi:10.1111/nph.12126.

Massman, W. J. (2000), A simple method for estimating frequency response corrections for eddy covariance systems, *Agric. For. Meteorol.*, *104*(3), 185–198, doi:10.1016/s0168-1923(00)00164-7.

Matheny, A. M., et al. (2014), Characterizing the diurnal patterns of errors in the prediction of evapotranspiration by several land-surface models: An NACP analysis, *J. Geophys. Res. Biogeosci.*, *119*, 1458–1473, doi:10.1002/2014JG002623.

Maurer, K. D., B. S. Hardiman, C. S. Vogel, and G. Bohrer (2013), Canopy-structure effects on surface roughness parameters: Observations in a Great Lakes mixed-deciduous forest, *Agric. For. Meteorol.*, *177*, 24–34, doi:10.1016/j.agrformet.2013.04.002.

McAdam, S. A. M., and T. J. Brodribb (2014), Separating active and passive influences on stomatal control of transpiration, *Plant Physiol.*, *164*, 1578–1586, doi:10.1104/pp.113.231944.

McCulloh, K. A., and J. S. Sperry (2005), Patterns in hydraulic architecture and their implications for transport efficiency, *Tree Physiol.*, *25*, 257–267.

McCulloh, K. A., D. M. Johnson, F. C. Meinzer, S. L. Voelker, B. Lachenbruch, and J.-C. Domec (2012), Hydraulic architecture of two species differing in wood density: Opposing strategies in co-occurring tropical pioneer trees, *Plant Cell Environ.*, *35*, 116–125, doi:10.1111/j.1365-3040.2011.02421.x.

McDowell, N., et al. (2008), Mechanisms of plant survival and mortality during drought: Why do some plants survive while others succumb to drought?, *New Phytol.*, *178*, 719–739, doi:10.1111/j.1469-8137.2008.02436.x.

McNaughton, K. G., and P. G. Jarvis (1986), Stomatal control of transpiration—Scaling up from leaf to region, *Adv. Ecol. Res.*, *15*, 1–49, doi:10.1016/s0065-2504(08)60119-1.

Miller, G. R., X. Y. Chen, Y. Rubin, S. Y. Ma, and D. D. Baldocchi (2010), Groundwater uptake by woody vegetation in a semiarid oak savanna, *Water Resour. Res.*, *46*, 14, doi:10.1029/2009WR008902.

Monteith, J. L. (1965), Evaporation and environment, *Symp. Soc. Exp. Biol.*, *19*, 205–234.

Moore, G. W., B. J. Bond, J. A. Jones, N. Phillips, and F. C. Meinzer (2004), Structural and compositional controls on transpiration in 40-and 450-year-old riparian forests in western Oregon, USA, *Tree Physiol.*, *24*, 481–491.

Morin, T. H., G. Bohrer, L. Naor-Azrieli, S. Mesi, W. T. Kenny, W. J. Mitsch, and K. V. R. Schäfer (2014), The seasonal and diurnal dynamics of methane flux at a created urban wetland, *Ecol. Civ Eng.*, doi:10.1016/j.ecoleng.2014.02.002.

Nadezhdina, N., J. Cermak, and R. Ceulemans (2002), Radial patterns of sap flow in woody stems of dominant and understory species: Scaling errors associated with positioning of sensors, *Tree Physiol.*, *22*(13), 907–918.

Nave, L. E., et al. (2011), Disturbance and the resilience of coupled carbon and nitrogen cycling in a north temperate forest, *J. Geophys. Res.*, *116*, G04016, doi:10.1029/2011JG001758.

Novick, K., S. Brantley, C. F. Miniat, J. Walker, and J. M. Vose (2014), Inferring the contribution of advection to total ecosystem scalar fluxes over a tall forest in complex terrain, *Agric. For. Meteorol.*, *185*, 1–13, doi:10.1016/j.agrformet.2013.10.010.

O'Brien, J. J., S. F. Oberbauer, and D. B. Clark (2004), Whole tree xylem sap flow responses to multiple environmental variables in a wet tropical forest, *Plant Cell Environ.*, *27*(5), 551–567, doi:10.1111/j.1365-3040.2003.01160.x.

O'Grady, A. P., D. Worledge, and M. Battaglia (2008), Constraints on transpiration of *Eucalyptus globulus* in southern Tasmania, Australia, *Agric. For. Meteorol.*, *148*, 453–465, doi:10.1016/j.agrformet.2007.10.006.

Oishi, A. C., R. Oren, and P. C. Stoy (2008), Estimating components of forest evapotranspiration: A footprint approach for scaling sap flux measurements, *Agric. For. Meteorol.*, *148*, 1719–1732, doi:10.1016/j.agrformet.2008.06.013.

Pan, Y., et al. (2011), A large and persistent carbon sink in the world's forests, *Science*, *333*, 988–993, doi:10.1126/science.1201609.

Pastor, J., J. D. Aber, C. A. McClaugherty, and J. M. Melillo (1982), Geology, soils and vegetation of Blackhawk Island, Wisconsin, *Am. Midl. Nat.*, *108*(2), 266–277, doi:10.2307/2425487.

Pearcy, R. W., J. R. Ehleringer, H. A. Mooney, and P. W. Rundel (Eds.) (1989), *Plant Physiological Ecology*, pp. 137–142, Chapman and Hall, New York.

Penman, H. L. (1948), Natural Evaporation from open water, bare soil and grass, *Proc. R. Soc. A*, *193*(1032), 120–145, doi:10.1098/rspa.1948.0037.

Phillips, N., and R. Oren (1998), A comparison of daily representations of canopy conductance based on two conditional time-averaging methods and the dependence of daily conductance on environmental factors, *Ann. Sci. For.*, *55*(1-2), 217–235, doi:10.1051/forest:19980113.

Phillips, N., R. Oren, and R. Zimmermann (1996), Radial patterns of xylem sap flow in non-, diffuse- and ring-porous tree species, *Plant Cell Environ.*, *19*(8), 983–990, doi:10.1111/j.1365-3040.1996.tb00463.x.

Reichstein, M., et al. (2005), On the separation of net ecosystem exchange into assimilation and ecosystem respiration: Review and improved algorithm, *Global Change Biol.*, *11*, 1424–1439, doi:10.1111/j.1365-2486.2005.001002.x.

Renninger, H. J., K. L. Clark, N. Skowronski, and K. V. R. Schafer (2013), Effects of a prescribed fire on water use and photosynthetic capacity of pitch pines, *Trees Struct Funct.*, *27*, 1115–1127, doi:10.1007/s00468-013-0861-5.

Royer, P. D., D. D. Breshears, C. B. Zou, N. S. Cobb, and S. A. Kurc (2010), Ecohydrological energy inputs in semiarid coniferous gradients: Responses to management- and drought-induced tree reductions, *For. Ecol. Manage.*, *260*, 1646–1655, doi:10.1016/j.foreco.2010.07.036.

Running, S. W., and J. C. Coughlan (1988), A general model of forest ecosystem processes for regional applications. 1. Hydrologic balance, canopy gas exchange and primary production processes, *Ecol. Modell.*, *42*(2), 125–154, doi:10.1016/0304-3800(88)90112-3.

Schäfer, K. V. R., R. Oren, and J. D. Tenhunen (2000), The effect of tree height on crown level stomatal conductance, *Plant Cell Environ.*, *23*(4), 365–375, doi:10.1046/j.1365-3040.2000.00553.x.

Schäfer, K. V. R., H. J. Renninger, K. L. Clark, and D. Medvigy (2013), Hydrological responses to defoliation and drought of an upland oak/pine forest, *Hydrol. Processes*, *28*, 6113–6123, doi:10.1002/hyp.10104.

Schäfer, K. V. R., H. J. Renninger, N. J. Carlo, and D. W. Vanderklein (2014), Forest response and recovery following disturbance in upland forests of the Atlantic Coastal Plain, *Front. Plant Sci.*, *5*, doi:10.3389/fpls.2014.00294.

Schmid, H. P., H. B. Su, C. S. Vogel, and P. S. Curtis (2003), Ecosystem-atmosphere exchange of carbon dioxide over a mixed hardwood forest in northern lower Michigan, *J. Geophys. Res.*, *108*(D14), 4417, doi:10.1029/2002JD003011.

Schnitzer, S. A., et al. (2012), Liana abundance, diversity, and distribution on Barro Colorado Island, Panama, *PLoS One*, *7*, e5214, doi:10.1371/journal.pone.0052114.

Sellers, P. J., M. D. Heiser, F. G. Hall, S. J. Goetz, D. E. Strebel, S. B. Verma, R. L. Desjardins, P. M. Schuepp, and J. I. MacPherson (1995), Effects of spatial variability in topography, vegetation cover and soil moisture on area-averaged surface fluxes: A case study using the FIFE 1989 data, *J. Geophys. Res.*, *100*(D12), 25,607–25,629, doi:10.1029/95JD02205.

Shinohara, Y., K. Tsuruta, A. Ogura, F. Noto, H. Komatsu, K. Otsuki, and T. Maruyama (2013), Azimuthal and radial variations in sap flux density and effects on stand-scale transpiration estimates in a Japanese cedar forest, *Tree Physiol.*, *33*, 550–558, doi:10.1093/treephys/tpt029.

Simard, M., E. N. Powell, K. F. Raffa, and M. G. Turner (2012), What explains landscape patterns of tree mortality caused by bark beetle outbreaks in Greater Yellowstone?, *Global Ecol. Biogeogr.*, *21*, 556–567, doi:10.1111/j.1466-8238.2011.00710.x.

Stannard, D. I. (1993), Comparison of Penman-Monteith, Shuttleworth-Wallace and modified Priestly-Taylor evapotranspiration models for wildland vegetation in semiarid rangeland, *Water Resour. Res.*, *29*(5), 1379–1392, doi:10.1029/93WR00333.

Stephens, S. L., J. J. Moghaddas, B. R. Hartsough, E. E. Y. Moghaddas, and N. E. Clinton (2009), Fuel treatment effects on stand-level carbon pools, treatment-related emissions, and fire risk in a Sierra Nevada mixed-conifer forest, *Can. J. For. Res.*, *39*, 1538–1547, doi:10.1139/x09-081.

Taneda, H., and J. S. Sperry (2008), A case-study of water transport in co-occurring ring- versus diffuse-porous trees: Contrasts in water-status, conducting capacity, cavitation and vessel refilling, *Tree Physiol.*, *28*, 1641–1651.

Thom, A. S. (1972), Momentum, mass and heat exchange of vegetation, *Q. J. R. Meteorol. Soc.*, *98*(415), 124–134, doi:10.1002/qj.49709841510.

Thompson, S. E., C. J. Harman, A. G. Konings, M. Sivapalan, A. Neal, and P. A. Troch (2011), Comparative hydrology across AmeriFlux sites: The variable roles of climate, vegetation, and groundwater, *Water Resour. Res.*, *47*, W00J07, doi:10.1029/2010WR009797.

Thomsen, J., G. Bohrer, A. M. Matheny, V. Y. Ivanov, L. He, H. Renninger, and K. Schäfer (2013), Contrasting hydraulic strategies during dry soil conditions in *Quercus rubra* and *Acer rubrum* in a sandy site in Michigan, *Forests*, *4*, 1106–1120.

Tyree, M. T., and J. S. Sperry (1989), Vulnerability of xylem to cavitation and embolism, *Annu. Rev. Plant Physiol. Plant Mol. Biol.*, *40*, 19–36.

Tyree, M. T., and M. H. Zimmermann (2002), Xylem structure and the ascent of sap, in *Xylem Structure and the Ascent of Sap*, edited by T. E. Timell, Springer, New York.

Unsworth, M. H., N. Phillips, T. Link, B. J. Bond, M. Falk, M. E. Harmon, T. M. Hinckley, D. Marks, and K. T. P. U (2004), Components and controls of water flux in an old-growth Douglas-fir-western hemlock ecosystem, *Ecosystems*, *7*, 468–481, doi:10.1007/s10021-004-0138-3.

Uriarte, M., J. S. Clark, J. K. Zimmerman, L. S. Comita, J. Forero-Montana, and J. Thompson (2012), Multidimensional trade-offs in species responses to disturbance: Implications for diversity in a subtropical forest, *Ecology*, *93*, 191–205.

Van Genuchten, M. T. (1980), A closed form equation for predicting the hydraulic conductivity of unsaturated soils, *Soil Sci. Soc. Am. J.*, *44*(5), 892–898.

Verbeeck, H., K. Steppe, N. Nadezhdina, M. O. De Beeck, G. Deckmyn, L. Meiresonne, R. Lemeur, J. Cermak, R. Ceulemans, and I. A. Janssens (2007a), Model analysis of the effects of atmospheric drivers on storage water use in Scots pine, *Biogeosciences*, *4*, 657–671.

Verbeeck, H., K. Steppe, N. Nadezhdina, M. Op de Beeck, G. Deckmyn, L. Meiresonne, R. Lemeur, J. Cermak, R. Ceulemans, and I. A. Janssens (2007b), Stored water use and transpiration in Scots pine: A modeling analysis with ANAFORE, *Tree Physiol.*, *27*, 1671–1685.

Webb, E. K., G. I. Pearman, and R. Leuning (1980), Correction of flux measurements for density effects due to heat and water-vapor transfer, *Q. J. R. Meteorol. Soc.*, *106*(447), 85–100, doi:10.1002/qj.49710644707.

Webster, C. R., and C. G. Lorimer (2003), Comparative growing space efficiency of four tree species in mixed conifer-hardwood forests, *For. Ecol. Manage.*, *177*(1-3), 361–377, doi:10.1016/s0378-1127(02)00394-8.

Weng, E. S., and Y. Q. Luo (2008), Soil hydrological properties regulate grassland ecosystem responses to multifactor global change: A modeling analysis, *J. Geophys. Res.*, *113*, G03003, doi:10.1029/2007JG000539.

Wu, Y. P., S. G. Liu, and O. I. Abdul-Aziz (2012), Hydrological effects of the increased CO_2 and climate change in the Upper Mississippi River Basin using a modified SWAT, *Clim. Change*, *110*, 977–1003, doi:10.1007/s10584-011-0087-8.

Wullschleger, S. D., R. J. Norby, and C. A. Gunderson (1992), Growth and maintenance respiration in leaves of *Liriodendron tulipifera L.* exposed to long-term carbon dioxide enrichment in the field, *New Phytol.*, *121*(4), 515–523, doi:10.1111/j.1469-8137.1992.tb01121.x.

Wullschleger, S. D., P. J. Hanson, and D. E. Todd (2001), Transpiration from a multi-species deciduous forest as estimated by xylem sap flow techniques, *For. Ecol. Manage.*, *143*(1-3), 205–213, doi:10.1016/s0378-1127(00)00518-1.

Zhang, Q., S. Manzoni, G. G. Katul, A. Porporato, and D. Yang (2014), The hysteretic evapotranspiration—Vapor pressure deficit relation, *J. Geophys. Res. Biogeosci.*, *119*, 125–140, doi:10.1002/2013JG002484.